Observation of Locked Intrinsic Localized Vibrational Modes in a Micromechanical Oscillator Array

Observation of Locked Intrinsic Localized Vibrational Modes in a Micromechanical Oscillator Array

M. Sato, B. E. Hubbard, and A. J. Sievers
Laboratory of Atomic and Solid State Physics, Cornell University, Ithaca, New York 14853-2501

B. Ilic
Cornell Nanofabrication Facility and Department of Applied and Engineering Physics, Cornell University, Ithaca, New York 14853-5403

D. A. Czaplewski and H. G. Craighead
Department of Applied and Engineering Physics, Cornell University, Ithaca, New York 14853-3501
(Received 23 August 2002; published 30 January 2003)

The nonlinear vibrational properties of a periodic micromechanical oscillator array have been measured. For sufficiently large amplitude of the driver, the optic mode of the di-element cantilever array becomes unstable and breaks up into excitations ranging over only a few cells. A driver-induced locking effect is observed to eternalize some of these intrinsic localized modes so that their amplitudes become fixed and the modes become spatially pinned.

DOI: 10.1103/PhysRevLett.90.044102 PACS numbers: 05.45.–a, 05.45.Xt, 63.20.Pw, 85.85.+j

Intrinsic localized modes (ILMs) which extend over only a few lattice sites of a periodic nonlinear lattice have been examined theoretically in a variety of systems [1–4]. Although the smallest excitations would be in a quantum lattice [5], there are still interesting issues in classical models to be explored experimentally such as mobility [6], discrete lattice potential [7], and interaction among ILMs [8], as well as the long-time behavior of a driver-induced modulational instability for a dissipative system. Thus the exploration of amplitude-dependent features is one of the important experimental issues at the present time.

Although some experimental studies have been reported for large scale mechanical systems [9], for somewhat smaller Josephson-junction arrays [10,11] and optical waveguides [12,13], and for nanoscale lattices [14–16] none of these systems are, as yet, appropriate for studying the detailed motion of large numbers of ILMs in the presence of a driver. Recently, micro-electro-mechanical system (MEMS) silicon technology has matured sufficiently [17] so that we can make a few hundred coupled cantilever oscillators [18]. In this Letter we describe our experimental investigation of ILM creation and locking for a cantilever array in the presence of damping, disorder, and a driver.

Our cantilever array is produced from a photoresist mask over a silicon nitride layer on a silicon substrate. This is exposed and then etched via a CF_4 plasma in a reactive ion chamber. The silicon substrate is undercut using an anisotropic KOH etch, thus releasing the silicon nitride cantilevers. A 3D rendition of one unit cell of the resulting array is shown in Fig. 1(a). Such cantilevers have a hard nonlinearity. To achieve the large amplitude uniform mode instability required to produce ILMs one needs to drive the highest frequency uniform mode of the system [19]. In order to accomplish this when using a piezoelectric transducer (PZT) driver, two different length cantilevers per unit cell have been constructed as shown in Fig. 1(a). With this di-element array the dispersion curve is folded over so that the highest frequency vibrational mode is now at the zone center. The room temperature quality factor of this mode is about 8000.

Figure 1(b) shows the experimental setup for measuring ILM dynamics and mobility versus time. A cylindrical lens is used to focus a He-Ne laser line image on the static array. The reflected beam is then incident on a 1-D CCD camera. The PZT is driven with a voltage controlled oscillator permitting frequency chirping [20] or cw operation. The switch, the ramp generator, and the computer are synchronized with the camera by using a pulse generator. The speed of the camera, about 18 kHz, is insufficient to monitor the sinusoidal motion of the cantilevers. However, as the vibration of a cantilever grows, the reflected laser beam increasingly misses the 1-D CCD camera and the image of that particular cantilever becomes darker. The speed of the camera is fast enough to observe the lateral motion of an ILM. This relatively straightforward observational method permits systematic monitoring of the excitation pattern of large amplitude ILMs and their interaction with a driver.

Figure 2 shows the room temperature cantilever excitation pattern versus time for a 248-element array. The CCD camera can image only a portion of the sample, about 220 cantilevers. The cantilever positions can be identified by the white lines to the left of time = 0. The pulse interval is highlighted. The high-power, PZT driver (~ 20 V) is chirped from $0.9986 f_0$ ($f_0 = 147.0$ kHz, the maximum resonant frequency of the upper band) to

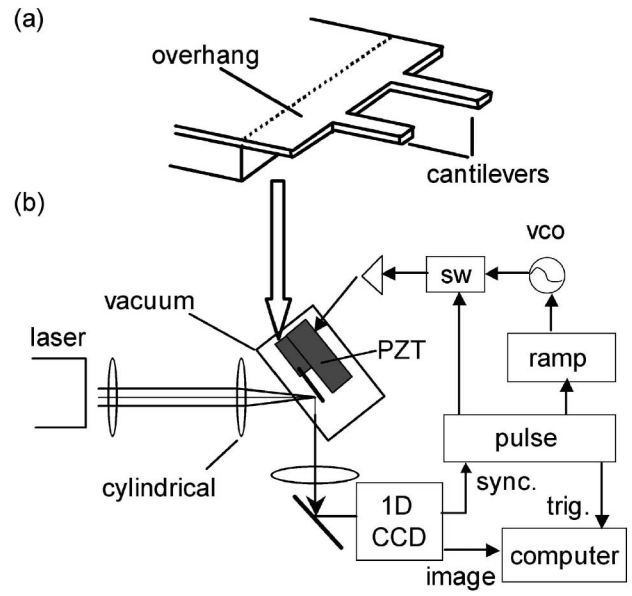

FIG. 1. (a) Schematic figure of a di-element type cantilever array. Cantilevers are made from a 300 nm thick Si_3N_4 film. The lengths of longer and shorter cantilevers are 55 and 50 μm, respectively. Width and pitch of cantilevers are 15 and 40 μm, respectively. (b) Experimental setup for the ILM measurement. A beam from a He-Ne laser is focused along the array by using a cylindrical lens. A 1-D CCD is used to detect the beam reflected by the cantilevers. A voltage controlled oscillator (vco), switch (sw), and amplifier are used to drive the PZT. The frequency of the vco is controlled by a ramp generator. A pulse generator, which controls the switch and the ramp generator, is synchronized to the camera. If the vibration of a cantilever is large, the deflection of the beam increases and the image at the cantilever site becomes dark.

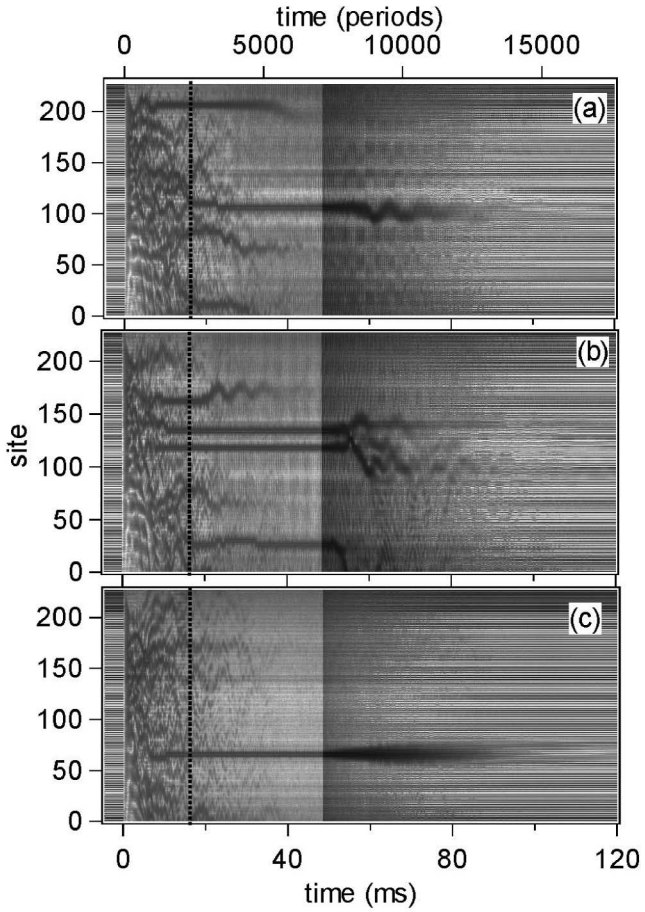

FIG. 2. Cantilever excitation versus time showing the production, pinning and decay of ILMs. Traces (a) and (b) are for a frequency chirp from $0.9986f_0$ (resonant frequency, $f_0 =$ 147.0 kHz) to $1.016f_0$, and trace (c) is for a chirp from $0.9986f_0$ to $1.034f_0$. The highlighted regions correspond to the time where the pulse is on. The pulse duration is 48.9 ms. The chirp ends at 16.2 ms (dotted line). The dark trajectories near the end of the chirp identify moving and stationary ILMs. After the chirp ends some ILMs die out while others remained pinned at a particular site. After the pulse ends all remaining ILMs die out.

$1.016f_0$ between time $= 0$ and 16.2 ms as indicated by the dotted vertical line in the figure. The experimental results shown in Figs. 2(a) and 2(b) are different, although the starting conditions are identical, which is to be expected for a process initiated by noise. The dark regions versus time identify the trajectories of large amplitude localized excitations. At early times ILMs form, move, oscillate and hop until the chirp ends (dotted lines). At longer times between 16.2 and 48.9 ms, when the driver is in the cw fixed frequency mode, those ILMs synchronous with the driver continue to receive energy while the others die out. These synchronous, large amplitude, ILMs become pinned. After the pulse, these stationary ILMs lose energy, become broader, break free from the pinning site, and sometimes oscillate about it before decaying. Figure 2(c) shows the results for a slightly different starting condition, where the driver frequency is chirped over a larger interval, $0.9986f_0$ to $1.034f_0$. As long as the chirping starts near the top of the band and ends $\sim$2–3% higher than f_0, the different chirping schemes give similar results. Interestingly, the number of stable ILMs depends on the detailed frequency path of the driver. Although not possible to see in this figure, other experiments show that the strongly excited pinned ILMs are centered only on the short cantilever sites, the high frequency vibrator of the di-element.

To simulate the dynamics of an array of cantilever beams that are coupled together by the overhang region between them, we ignore the dynamics of the overhang and assume it acts only as a massless coupler between cantilevers. For the large amplitude problem of interest, each cantilever is then represented by a mass and an on-site potential which has both harmonic (quadratic) and anharmonic (hard quartic) terms. The coupling between cantilevers is taken to be harmonic for all cantilever amplitudes. With such a model, the equations of motion for a unit cell become

$$m_a \frac{d^2}{dt^2} x_{ai} + \frac{m_a}{\tau} \frac{d}{dt} x_{ai} + k_{2a} x_{ai} + k_{4a} x_{ai}^3 + k_I (2x_{ai} - x_{bi} - x_{bi-1}) = m_a \alpha \quad (1)$$

and

$$m_b \frac{d^2}{dt^2} x_{bi} + \frac{m_b}{\tau} \frac{d}{dt} x_{bi} + k_{2b} x_{bi} + k_{4b} x_{bi}^3 + k_I (2x_{bi} - x_{ai+1} - x_{ai}) = m_b \alpha, \quad (2)$$

where x_{ai} and x_{bi} represent displacements of the cantilever ends, m_a and m_b are their masses, τ is an energy lifetime, k_{2a} and k_{2b} are the on-site harmonic spring constants, k_{4a} and k_{4b} are on-site quartic spring constants, and k_I is the harmonic coupling constant. Since the PZT is bonded to the sample each cantilever feels a common acceleration, α. The dispersion curve for our system is obtained from linearized Eqs. (1) and (2). The three free parameters (k_{2a}, k_{2b}, k_I) are chosen to give a good fit to the upper branch of the experimental dispersion curve. The values of the on-site quartic spring constants (k_{4a}, k_{4b}) are adjusted so that the upper branch frequency in the simulation shows the same frequency shift as observed in the experiment. The τ is determined from the linear amplitude decay measurement. The parameters are given in the caption of Fig. 3.

In the simulation the system is initialized with a small amount of random noise, which will ultimately act to perturb the highly excited uniform mode and hence trigger the modulational instability. The driver frequency starts at the top of the upper band, then continuously increases linearly to a frequency $1.029 f_0$ over a time interval of 2500 periods. Next, the driver frequency is kept at $1.029 f_0$ until time = 7500 periods at which point it is turned off.

Figure 3(a) shows an energy density versus time plot for a particular simulation result. The total number of cantilevers is 250 with fixed-end boundary conditions. There is no qualitative difference between simulations with the periodic- and fixed-end boundary conditions except near the boundaries. As with experiment, the entire array is excited uniformly. During the chirping phase, many ILMs of different strengths appear as shown in the figure (strength = darkness). Strong ones are nearly pinned and hop from site to site while weaker ones move easily through the lattice. Many of the ILMs die out after ~1000 periods of oscillation. In this particular simulation, one ILM clearly persists much longer than the others. It is identified in Fig. 3(a) as a locked ILM since its frequency is locked to the driver frequency [21]. This locking prevents it from decaying like all the other ILMs. Other ILMs identified with the oval at the top of the figure, fail to frequency lock, and hence ultimately decay after a time lapse of about 3000 periods. The reflection of a running mode by the locked ILM illustrates the rigidity of such a locked state. (For no driver and a nondissipative system a small amplitude running mode is absorbed by the driver [19].) Once the driver is turned off, the locked ILM decays peacefully, maintaining the symmetry of the mode without further motion in the lattice. This result is similar to that shown in experiment in Fig. 2(c), although it should be added that it is much easier to produce locked ILMs in experiment than in simulations. Figure 3(b) shows another simulation of energy density versus time. In this particular example, four modes can be identified that persist much longer than the others. Three of these are found to have their frequency locked to the driver. Even though the fourth one, another large amplitude ILM, persists after the end of the chirp it still fails to lock to the frequency of the driver, and hence ultimately

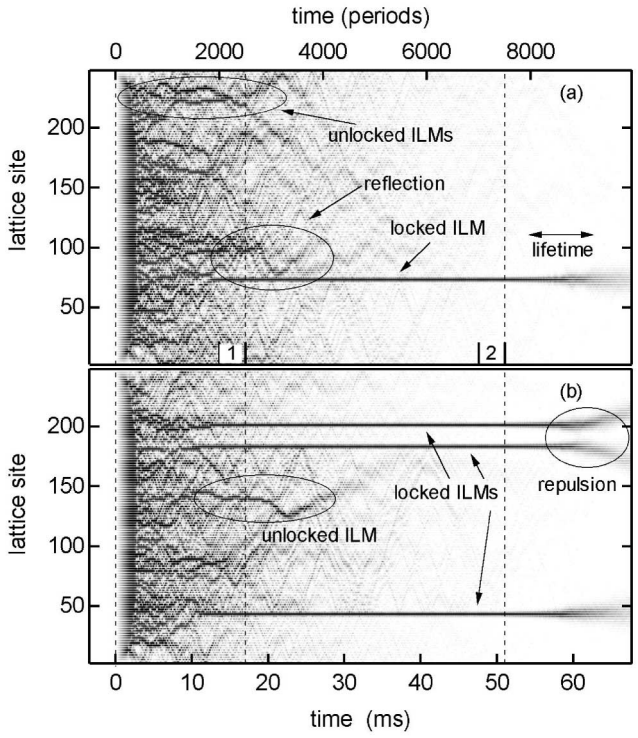

FIG. 3. Computer simulations of ILM production, locking, and decay. The driver frequency starts from f_0, the top of the upper dispersion band, increases up to $1.029 f_0$ linearly until the 2500th periods, first dashed interval, and then is held there during the remainder of the pulse, until 7500 periods. (a) Energy density versus time. Dark trajectories during the chirp identify ILMs. The ellipses identify particular processes. The one pinned ILM which is seen during the cw pulse region is frequency locked to the driver. The horizontal arrow shows the energy lifetime (8.75 ms) used in this simulation. (b) Energy density versus time for the same starting condition as in (a), except for the initial random noise distribution. Three locked ILMs are identified. The ellipses identify the decay of an unlocked ILM and the repulsion of two ILMs, respectively. Parameters are $m_a = 5.46 \times 10^{-13}$ kg, $m_b = 4.96 \times 10^{-13}$ kg, $\tau = 8.75$ ms, $k_{2a} = 0.303$ kg/s^2, $k_{2b} = 0.353$ kg/s^2, $k_I = 0.0241$ kg/s^2, $k_{4a} = k_{4b} = 5.0 \times 10^8$ kg/s^{2}m^2, and $\alpha = 1.0 \times 10^4$ m/s^2.

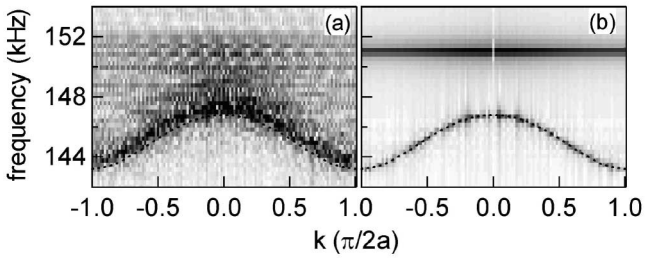

FIG. 4. Simulated production, locking, and decay of ILMs in k space. Time-space Fourier transform of the displacement for the 500 period time windows identified in Fig. 3(a): They are at (i) 2000 and (ii) 7000 periods, respectively. Frame (a) shows the time development at the end of the chirp and (b), at the end of the locked state. For reference the linear dispersion curve of the upper band is shown (dotted).

decays. The two neighboring locked ILMs are close enough together that their interaction can be observed once the pulse is off and the decay begins.

To examine the development of such locked ILMs from another view the double Fourier transform of the cantilever motion shown in Fig. 3(a) is taken over specific time intervals, identified by the two numbers at the bottom of that frame. The resulting time evolution of (ω, k) excitation plots is shown in Figs. 4(a) and 4(b). The dotted curves in these figures represent the position of the upper branch of the linear dispersion curve for the di-element cantilever array. Figure 4(a) is a time interval at the end of the chirp. Several insipient ILMs emerge in the k-space representation. The late stage of the locked state is shown in Fig. 4(b) where a monochromatic locked mode appears.

Our experimental technique, which images and records the time dependent vibration envelope of a di-element micromechanical oscillator array in the presence of a chirped driver, shows the evolution of the unstable uniform mode into ILMs. Initially traveling ILMs are created but finally these modes are pinned at an individual lattice site. The fact that nearly identical experimental starting conditions give completely different localized pinning sites in Figs. 2(a)–2(c) strongly supports our claim that the localized excitations in the cantilever array are ILMs, not impurity-induced localized modes. From our simulations, it is found that these same spatially pinned ILMs are frequency locked to the driver so that their amplitudes, which in the unlocked state can have any value, now become fixed. More generally, our experiments show that such locked ILMs are a robust feature of a driven nonlinear periodic system with damping and it is to be expected that such monochromatic ILMs could also be produced in the nonlinear low lying excitations of atomic lattices.

We thank L. Q. English and J. P. Sethna for helpful discussions. Supported in part by NSF-DMR and by the Cornell Center of Materials Research. The sample fabrication was performed at the Cornell Nanofabrication Facility.

[1] S. A. Kiselev, S. R. Bickham, and A. J. Sievers, Comments Condens. Matter Phys. **17**, 135 (1995).
[2] S. Flach and C. R. Willis, Phys. Rep. **295**, 181 (1998).
[3] R. Lai and A. J. Sievers, Phys. Rep. **314**, 147 (1999).
[4] P. G. Kevrekidis, K. Ø. Rasmussen, and A. R. Bishop, Int. J. Mod. Phys. B **15**, 2833 (2001).
[5] W. Z. Wang, A. R. Bishop, J. T. Gammel, and R. N. Silver, Phys. Rev. Lett. **80**, 3284 (1998).
[6] O. Bang and M. Peyrard, Physica (Amsterdam) **81D**, 9 (1995).
[7] Y. S. Kivshar and D. K. Campbell, Phys. Rev. E **48**, 3077 (1993).
[8] M. Johansson and S. Aubry, Phys. Rev. E **61**, 5864 (2000).
[9] S. Lou and G. Huang, Mod. Phys. Lett. B **9**, 1231 (1995).
[10] E. Trias, J. J. Mazo, and T. P. Orlando, Phys. Rev. Lett. **84**, 741 (2000).
[11] P. Binder, D. Abraimov, A. V. Ustinov, S. Flach, and Y. Zolotaryuk, Phys. Rev. Lett. **84**, 745 (2000).
[12] H. S. Eisenberg, Y. Silberberg, R. Morandotti, A. R. Boyd, and J. S. Aitchison, Phys. Rev. Lett. **81**, 3383 (1998).
[13] R. Morandotti, U. Peschel, J. S. Aitchison, H. S. Eisenberg, and Y. Silberberg, Phys. Rev. Lett. **83**, 2726 (1999).
[14] B. I. Swanson, L. A. Brozik, S. P. Love, G. F. Strouse, A. P. Shreve, A. R. Bishop, W.-Z. Wang, and M. I. Salkola, Phys. Rev. Lett. **82**, 3288 (1999).
[15] U. T. Schwarz, L. Q. English, and A. J. Sievers, Phys. Rev. Lett. **83**, 223 (1999).
[16] M. Sato, L. Q. English, B. E. Hubbard, and A. J. Sievers, J. Appl. Phys. **91**, 8676 (2002).
[17] D. J. Bishop, C. R. Giles, and S. R. Das, Sci. Am. **284**, 88 (2001).
[18] M. Zalalutdinov, B. Ilic, D. Czaplewski, A. Zehnder, H. G. Craighead, and J. M. Parpia, Appl. Phys. Lett. **77**, 3287 (2000).
[19] M. Peyrard, Physica (Amsterdam) **119D**, 184 (1998).
[20] T. Rössler and J. B. Page, Phys. Rev. B **62**, 11 460 (2000).
[21] T. Rössler and J. B. Page, Phys. Lett. A **204**, 418 (1995).